Published in final edited form as:
Chem Soc Rev. 2010 March ; 39(3): 912–922. doi:10.1039/b822556g.

Nanofluidic concentration devices for biomolecules utilizing ion concentration polarization: theory, fabrication, and applications

Sung Jae Kim[1], **Yong-Ak Song**[1], and **Jongyoon Han**[1,2,*]

[1]Department of Electrical Engineering and Computer Science, Massachusetts Institute of Technology, 77 Massachusetts Avenue, Cambridge, MA 02139, USA

[2]Department of Biological Engineering, Massachusetts Institute of Technology, 77 Massachusetts Avenue, Cambridge, MA 02139, USA

Abstract

Recently, a new type of electrokinetic concentration devices has been developed in a microfluidic chip format, which allows efficient trapping and concentration of biomolecules by utilizing ion concentration polarization near nanofluidic structures. These devices have drawn much attention not only due to their potential application in biomolecule sensing, but also due to the rich scientific content related to ion concentration polarization, the underlying physical phenomenon for the operation of these electrokinetic concentration devices. This tutorial review provides an introduction to the scientific and engineering advances achieved, in-depth discussion about several interesting applications of these unique concentration devices, and their current limitations and challenges.

1. Introduction

For molecular detection and analysis in microfluidic systems, efficient sample collection/preconcentration methods are necessary in order to achieve the full potential of any sensing schemes used. Lowering the detection limit is highly desirable in biomolecule sensing, in order to diagnose hard to-treat diseases earlier (when biomarker concentrations are lower than the detection limit of a given sensor) or to detect potentially harmful (bio) chemical agents well below the level where they can present significant danger. In many of these chemical and biological sensing applications, the key issue is often not the total amount of molecules available for the sensing, but the low concentrations of these molecules present in the given sample. In such cases, a device that can collect molecules from a dilute sample with a sample volume of 1–100 μL and concentrate them into a smaller volume (nLBpL) sample bolus would have significant value. Such a device would also be meaningful for microfluidic chip-to world interfacing, since microfluidic devices are ideally suited for accurate manipulation and analysis of small fluid volumes (nL~pL), while existing pipetting technique allows handling and transferring of sample volumes larger than ~1 μL.

In response to this critical need, many research groups have introduced various concentration devices for biomolecules that utilize electrokinetic trapping,[1–3] field amplification stacking,[4] isoelectric focusing,[5] capillary electrophoresis, isotachophoresis,[6] affinity-based extraction[7] and membrane filtration.[8, 9] Among these techniques, this tutorial review focuses on `electrokinetic' concentration devices[1–3] that utilize ion concentration polarization (ICP). While these concentration devices are by no means the only concentration systems for biomolecules available, there are several unique characteristics of these devices that enable

*Correspondence should be addressed to Jongyoon Han: jyhan@mit.edu; phone: +1-617-253-2290; fax: +1-617-258-5846..

their use as a `generic' molecular concentrator. Unlike affinity-based concentration systems, these devices allow concentration regardless of the chemistry (hydrophobicity or binding characteristics) of the molecules involved. It is a field-addressable (electrokinetically driven) molecular trapping system, which allows efficient concentration and release of collected molecules, without suffering from clogging as in most size-based molecular concentration devices. If properly engineered, it is expected that these electrokinetic concentration devices would enhance various biosensing systems' detection sensitivity significantly.

Aside from its potential use in biosensing, these nanofluidic concentration devices have drawn significant interest from the purely scientific perspective. Even though ICP, the basic physical phenomenon behind the operation of the concentration devices, has been known for more than 100 years, the subject matter is still at the forefront of ongoing scientific research. In ICP, chemical (ion) diffusion, drift, and (nonlinear electrokinetic) fluid flow in the system are tightly coupled with each other. Therefore, the Poisson's equation, the Nernst–Planck equation and the Navier–Stokes equation have to be solved concurrently. In addition, ICP typically involves widely different scales of length (from (micro/)macro-size reservoirs to microchannels and nanochannels/nanopores), a nonlinear concentration gradient (bulk ion concentration to depleted, near-zero ion concentration), and changing electric fields. Most importantly, ICP is occurring at the macro/micro–nano interface, which means that usual approximations often used in microfluidic modeling may not be valid. For example, it is customary to assume a small electrical double layer thickness (Debye length λ_D<<system dimension) and therefore a single, constant zeta potential value in most microfluidic flow modeling. However, such an approximation would not be possible for ICP modeling, because of dynamic changes in local ion concentrations involved, as well as the inherently multi-scale nature of the system used. The facts mentioned above make ICP and its related phenomena an extremely challenging modeling problem. With these obvious scientific challenges, the investigation of ICP and its related phenomena are of critical importance in many engineering fields. ICP is one of the fundamental membrane transport phenomena, and understanding and even manipulating ICP could potentially lead to more efficient membrane systems for fuel cells and batteries. For studying this complicated, strongly coupled phenomenon at the micro–nano interface, the advent of microfluidic model systems,[10] as experimental platforms, opens up new exciting opportunities. In this tutorial review, which is intended to be an introductory review even for non-experts, we will begin by explaining the scientific background of the ICP. Then, we will review various existing fabrication methods to realize nanofluidic concentration devices utilizing microfluidic ICP. Finally, we will discuss some applications of the nanofluidic concentration devices in microfluidic assay systems and conclude this review with a discussion about their limitations and challenges. We would like to seek understanding from researchers whose important contributions in the field have been neglected here due to space limitation.

2. Science behind the nanofluidic molecular concentrator

2.1 Ion concentration polarization/ion depletion (enrichment) phenomena

The underlying mechanism for nanofluidic concentrators, is the ICP. It is one of the fundamental electrochemical transport phenomena that have been observed at nanoporous membranes.[11, 12] Nanoporous membranes with non-engineered pores can exhibit perm-selectivity (preferentially conducting ions with one polarity over another) when their dimensions become comparable with the thickness of the electrical double layer (EDL). The EDL is in the order of a few nanometers under uniform surface charge distributions and electrolyte concentration of physiological buffers.[3, 11] In these nanoporous structures, the EDL can overlap under moderate electrolyte concentration (<10 mM), resulting in a sheath of mobile `counterions' screening and shielding fixed (immobile) charges on the wall of nanopores/membrane materials. In such cases, counter-ions (to the nanopore's surface charges) can be transported through the nanopores (either by drift or diffusion), while `co-ions' (ions with the

same polarity as the surface charges) cannot due to electrostatic repulsion. The same phenomenon can be found in the ion transport process across ion-exchange membranes such as Nafion®, a widely used ion-selective membrane material with strongly negatively charged sulfonic groups, for fuel cells. As illustrated in Fig. 1, the perm-selective nanoporous membrane (usually with negatively charged surface on the pore wall) can be conceptually considered as a cation-selective ion conductor, with near-zero permeability to co-ionic species (anions). The fluxes of each ion, $N^{\pm}$, are the summation of a diffusive component resulting from the concentration gradient (∇c) and a drift term from the electric field (**E**),[11] which are given by

$$\mathbf{N}^{\pm}=\mathbf{N}^{\pm}_{diff}+\mathbf{N}^{\pm}_{drift}=-D_{\pm}\nabla c^{\pm}-c^{\pm}\mu_{\pm}\mathbf{E}. \quad (1)$$

Here $D^{\pm}$ denotes the diffusivities, $c^{\pm}$ is the ionic concentrations, and $\mu^{\pm}$ is the electrophoretic mobilities for positive and negative ions, respectively. Under a dc bias, cations can enter and pass through the cation-permselective membrane on the anodic side, while anions on the cathodic side would be hindered from entering the permselective membrane. Thus, a non-zero flux of cation can be maintained through the entire system, while the overall anion flux should be (near) zero. (A similar situation can be found near the electrolyte–electrode interface.) As a result, charge carriers that do not participate in conduction through the bulk/nano interface would either get accumulated or depleted. However, due to the strong electrostatic interaction between any unscreened ions, concentration of both positive and negative ions will be affected, leading to ion concentration gradients. In the steady state, ion concentrations on both sides of the membrane shift either higher (on the cathodic side) or lower (on the anodic side), depending on the amount of ion current going through the membrane.

While ICP has been known and observed in nanoporous membranes for a long time, scientific study of this phenomenon was hampered by the fact that the detailed structural parameters of these membranes are either not known or difficult to determine. However, advances in the nanochannel fabrication techniques[13, 14] enabled robust and controllable fabrication of regular-shaped nanochannels with similar spatial dimensions as the EDL, which is a requirement for perm-selective membranes. In these systems, ion and molecular transport properties can be studied and modeled more accurately. Pu et al. first experimentally demonstrated the ion enrichment/depletion phenomenon with planar nanochannels as a perm-selective membrane.[15] They observed that ion depletion/ion enrichment could take place up to a buffer concentration of 3 mM. Using a similar microfabricated micro/nanofluidic channel system, Kim et al. recently reported that the ion depletion was obtained at an even higher buffer concentration of 15 mM, in a 40 nm silicon nanofluidic channel, which corresponds to only ~3 nm double layer thickness.[10] At higher buffer concentrations above 15 mM, ICP can still occur depending on the bias and other parameters. This result clearly demonstrates that the equilibrium EDL thickness alone cannot adequately describe the phenomenon properly, mainly because ICP is a non-equilibrium phenomenon. Even when the EDL is not `thick' enough to cover the entire nanochannel depth, surface ion current (due to conduction in a `thin' EDL) through such a channel could induce a small amount of additional counter-ions transport, initiating a small concentration polarization (depletion and enrichment) This will in turn lead to increased permselectivity of the nanochannel, initiating a positive-feedback toward a full initiation of ICP even at moderate or high (~100 mM) ionic strength conditions. More recently, theoretical and experimental work by Santiago and co-workers concluded that the inverse Dukhin number, which is the ratio of bulk conductivity to the EDL conductivity, plays a deterministic role for ICP initiation, even under the conditions of a non-overlapped EDL.[16] It is able to explain that a highly charged nanojunction such as Nafion or a hydrogel polymeric nanojunction can trigger ICP in even higher ionic strength solutions, such as seawater (500 mM).

In the classical ICP theory,[11] originally developed by Nernst about 100 years ago, a fixed concentration boundary condition is defined, at a fixed distance from the membrane. This distance (often called the diffusion length) is typically considered as the distance scale pertinent to the bulk convective mixing. In other words, beyond the diffusion length from the nanojunctions, concentration gradients generated by ICP will be completely eliminated due to convective mixing in the bulk solution. Within the diffusion length, however, convective mixing was previously regarded as negligible, which led to a linear concentration gradient. However, while this classical theory qualitatively agrees with the experimental behavior in micro/nanofluidic systems, there are notable discrepancies. First, the concentration profile inside the ion depletion zone is not linear at all,[17] nor is the length scale of the depletion zone (the diffusion length) constant. Indeed, typical experimental behavior observed in ICP near nanochannels shows quite dynamic behaviors, often the depletion zone extends over quite a distance (a few millimetres, often all the way back to the reservoirs) depending on the applied electric field, buffer concentration, surface charges, etc. This is partly due to the fact that bulk convective mixing is significantly suppressed in microfluidic channels. Thus, a direct application of the classical ICP theory to the micro/nanofluidic experimental situations would be inadequate. It seems that any theory or modeling on ICP (and related molecular concentration devices) should include modeling of the local flow caused by ICP,[10, 18] due to its significant impact on the local ion concentration distribution.

2.2 Operation of the nanofluidic molecular concentrator

While there have been several types of nanofluidic concentrator developed during the past couple of years,[3, 19, 20] the basic mechanisms employed in these systems are identical. There are two common design variations, a single-gated and dual-gated system either with one or two nanojunctions to the neighboring microchannels, The single-gated concentration system with its simpler design consists of two parallel microchannels connected with a nanojunction, as shown in Fig. 2. With the equal voltages ($V_1 = V_2$) on the anodic side of the microchannel, the electric field through the nanojunction ($\mathbf{E}_N$) generates the ion depletion region and this region symmetrically propagates towards each reservoir, while the cathodic side microchannel is electrically grounded. This enrichment on the cathodic side could be and has been used as a concentration mechanism,[2] although the molecular concentration on this side tends to saturate and stop eventually. For more efficient concentration, one can use the anodic side depletion as a molecular trapping mechanism.[1, 3] By applying a voltage difference ($V_1 > V_2$) at the anodic side of the microchannel, one can generate a tangential electric field ($\mathbf{E}_T$) along the anodic side microchannel. This field would generate electroosmotic flow (EOF) through the microchannel to bring the target molecules into the region, where they will get trapped by the ICP maintained by the perm-selective current through the junction.[3] Alternatively, instead of applying $\mathbf{E}_T$, concentration systems utilizing the external pressure-driven flow at one end of the anodic microchannel can also be conceived.[1] In the electrokinetic operation of a nanofluidic concentration device,[3] $\mathbf{E}_T$ and $\mathbf{E}_N$ should be carefully chosen depending on the microchannel dimensions and buffer concentration. Since $\mathbf{E}_N$ mainly governs the electrokinetic situation inside the depletion zone, especially strong vortex-like flow (to be explained in the next section), it affects the stability of the concentration process significantly. Setting $\mathbf{E}_N$ too high can destroy the accumulated plug and induce an ever-expanding depletion region, decreasing the overall efficiency of the concentration process. $\mathbf{E}_T$ drives the electroosmotic fluid motion through the microchannel, so the accumulation speed increases with higher $\mathbf{E}_T$. However, if $\mathbf{E}_T$ is set too high, the plug starts to leak through the ion depletion zone. For stable concentration process, $V_2 > V_1/2$ is usually recommended. Since these two parameters are strongly coupled, they have to be optimized simultaneously ($\mathbf{E}_T$ for fast collection and $\mathbf{E}_N$ for stable operation). Preventing the plug receding could be achieved by either decreasing $\mathbf{E}_N$ or increasing $\mathbf{E}_T$ in an automated fashion, e.g., by using computer-aided controls combined with real time image analysis. Typical range for V_1 and V_2 are between 5 V and 50 V so that $\mathbf{E}_N$ is between 10 V

cm^{-1} and 100 V cm^{-1}, while $\mathbf{E}_T$ has a value of 5 V cm^{-1}–50 V cm^{-1} assuming a 1 cm long microchannel. The stability and efficiency of the concentration are also critically affected by the local flow, to be discussed in the next section.

2.3 Nonlinear electrokinetic flow and related phenomena

For engineering an optimized nanofluidic molecular concentrator, it is important to appreciate the complexity caused by a non-uniform concentration distribution and electric field in the system. The ion current (cation flux) through the membrane will saturate (stop increasing further) at the point when the ion concentration near the anodic side of the membrane becomes zero. This is often called the limiting current behavior.[11] This will make the current–voltage behavior of the membrane junction significantly deviate from that of Ohm's law. At sufficiently low electric potential, the current–voltage behavior still follows Ohm's law, since the ICP is not generated and there is no ion concentration gradient. By increasing the applied electric potential, however, the ion concentration at the anodic side of the nanojunction starts to decrease, and the system reaches a limiting current regime. Such an ion concentration gradient near the limiting current regime induces significant changes in the local conductivity and electric field distribution. Lower ionic strength within the depletion zone means that local ion conductivity will be lower, which can in turn render the local electric field significantly higher than the value predicted by Ohm's law. This has been experimentally confirmed via in situ measurement of local potential drop (directly related to local **E**) inside the depletion zone from embedded microelectrodes.[18] The electric field inside the ion depletion region was amplified more than 30-fold compared to outside of the depletion zone. The amplified electrokinetic flow and particle motions were also experimentally monitored using photobleaching and particle tracking method. Once ICP is triggered, electrokinetic motions (electrophoresis and electroosmosis) were significantly amplified along the entire microchannel due to high local electric field inside the ion depletion zone and high local zeta potential (ζ, caused by low ionic strength). One tangible consequence of these `amplified' electrokinetic responses is that the resulting fluid velocity through the microchannel can be much higher than that of equilibrium EOF at the same applied voltages. This amplified electrokinetic flow would give a clue that can explain the efficient concentration of peptides and protein more than one-million fold.[3] Previously, Tallarek and co-workers' one-dimensional simulation and experiments also supported the idea that local electric fields inside the ion depletion zone can be much greater than one in the bulk phase.[21] Therefore, one cannot simply use Ohm's law to predict the electric field and potential distribution within the system, and the zeta potential ζ, ion conductivity σ, and the local electric field **E** of the system are all coupled to the concentration profiles of the system, which is also dynamically changing. Theoretical understanding of these complex fluid flow patterns near the perm-selective nanopores/membranes is an active area of research. Rubinstein and co-workers theoretically suggested that there is a strong convective mixing created by the amplified electrokinetic response of the fluid layer right next to the membrane.[22] The amplification of electrokinetic responses can be induced because of the significantly high electric field inside the ion depletion zone, and therefore higher local zeta potential. Rubinstein derived the two-dimensional non-equilibrium electroosmotic slip boundary condition through a flat ion exchange membrane along with the linear stability as follows:

$$\mathbf{u}|_s - |\mathbf{E}|^2/8 \times \left(\partial^2 c/\partial x \partial y\right) / (\partial c/\partial y) \tag{2}$$

where **u** is fluid velocity, and *x* and *y* are the axes parallel and perpendicular to the ion-exchange membrane, respectively. This boundary condition mathematically imposed the strong and vortex-like circulation flow field near the membrane, as shown in Fig. 3a. The strong, non-linear EOF was initially observed in the experiments using ion-selective granules[23] and then later using an ion-selective membrane[24] (Fig. 3b). Further investigation of electroosmotic slip

and instability predicted that the electroosmotic velocity is proportional to the cube of the applied voltage at moderate strength, while the square relationship is still valid in large applied voltages.[25] Later on, Kim et al. reported the experimental, microscopic study on nonlinear electrokinetic flow generated near microfabricated nanochannels.[10, 18] They visualized the electrokinetic flow patterns inside and outside the ion-depletion region by tracking the fluorescent nanoparticles and dye molecules in situ, as shown in Fig. 3c and d. The speed of the circulating flow was estimated to be at least 10 times higher than that of equilibrium EOF expressed by the Smoluchowski formula under the same electrical potential distribution. While an interesting question about "over-limiting current" behavior associated with strong vortical flows would arise, it is out of the scope of this review and one can find related theories in other literature.[10, 24]

2.4 Engineering and modeling of the molecular concentrator

As previously mentioned, detailed engineering modeling of the ICP and molecular concentration device has not yet been achieved due to the numerous technical challenges. Excellent progress has been made recently, however, in elucidating the nature of local nonlinear electrokinetic flow near permselective membranes, and for better understanding and optimization of the nanofluidic concentrator.[17, 22, 26] Prior studies have shown that for dimension scales larger than 5 nm, continuum dynamics is still valid and gives a precise description of ion transports and fluid flows.[17, 26] The complete set of governing equations associated with convective electrodiffusion of ions in incompressible Newtonian electrolyte solutions and confined within micro/nanochannels is shown below:

$$\text{Fluid motions (Navier–Stokes equation):}\quad \partial\mathbf{u}/\partial t+(\mathbf{u}\cdot\nabla)\,\mathbf{u}=\mu\nabla^2\mathbf{u}-\nabla p+\rho_e\mathbf{E},\quad \nabla\cdot\mathbf{u}=0. \tag{3}$$

$$\text{Electric potential (Possion equation):}\quad \rho_e=\epsilon\nabla^2\square. \tag{4}$$

$$\text{Ion transport (Nernst–Planck equation):}\quad \partial c^{\pm}/\partial t=D_{\pm}\nabla\cdot(\nabla c^{\pm}\pm c^{\pm}\nabla\phi)-Pe\,(\mathbf{u}\cdot\nabla)\,c^{\pm}. \tag{5}$$

Here, p and ε are the external pressure and permittivity of the solution and *Pe* is the Peclet number which represents the ratio of mass transported by convection to mass transported by diffusion: $|\mathbf{u}|L/D\pm$ where L is the characteristic length of the system. Though *Pe* is usually quite large in most engineering applications (convection-dominant system), it is often small (diffusion-dominant system) or co-exists in the system of short length scale such as microfluidic applications and, thus, the system response can be greatly different depending on *Pe*.

Utilizing the mathematical models, a number of studies dealing with the direct simulation of ICP phenomena were reported with the aid of advanced numerical methods. Jin et al. conducted two-dimensional numerical simulations in micro–nanofluidic interconnect structures.[17] They captured the nonlinear electrokinetic behavior due to the induced pressure, vortex-like second kind of EOF for both positive and negative bias potentials. Huang and co-worker analyzed the shape of the depletion boundary (flat shape vs. parabolic shape) according to the depth of the

microchannel.[27] It obviously provided potential supporting information for the role of convective flow inside the depletion zone.

3. Fabrication of the molecular concentrator

Realization of nanofluidic molecular concentration devices involves a fabrication and integration of nanoscale fluidic features (either nanopores or nanochannels), which provides perm-selective junctions, to microscale channels. Earlier implementation of the device required expensive nanochannel fabrication techniques, but recently several inexpensive, straightforward approaches have been developed for fabricating ion-selective membrane junctions inside the microfluidic chip. These fabrication strategies can be grouped based on the materials used for the fabrication of concentrator chips, which are summarized in Fig. 4. Each method has its own advantages and disadvantages (summarized in Table 1), which should be carefully considered before selecting the method for any given device. The most common materials for microfluidic chips are silicon and poly(dimethylsiloxane) (PDMS).

3.1 Si-based fabrication of nanochannels

The first silicon preconcentrator device reported was built using standard photolithography and reactive ion etching (RIE) on silicon wafers, followed by wafer bonding to seal the microfluidic channels.3 After patterning the 5–20 μm wide nanochannels with standard lithography tools, the wafer was etched for ~10 s to a channel depth of 40 nm at which the EDL are overlapping. After the RIE etching, KOH etching was used to etch through the loading holes. Then, thermal oxidation was performed after stripping off the nitride to obtain proper electrical insulation. The bottom side was bonded with a Pyrex wafer using anodic bonding techniques. The schematic of the fabrication as well as images of a planar silicon nanochannel are shown in Fig. 5a. The dual-gated preconcentrator consists of two microfluidic channels (a few tens of μm in dimension) bridged by a nanofluidic channel as thin as 40 nm, as shown in Fig. 5b. At moderate buffer concentrations (~10 mM), the Debye layer thickness within a nanofluidic channel is not negligible and the nanofluidic channel becomes perm-selective when an electric field ($\mathbf{E}_N$) is applied across the nanochannel. For a negatively charged surface such as SiO_2, the resulting ion current will preferentially transfer positively charged counter-ions over the negatively charged co-ions. Past study has shown that a dual-gated design provides a more stable and consistent performance in preconcentration. A dual-gated preconcentration device in silicon-glass is shown in Fig. 5c. To increase the ion flux, a fabrication strategy has recently been developed that enables building multiple high-aspect-ratio nanochannels with a gap size of ~50 nm at a depth of ~40 μm[14] (Fig. 6). The novel idea behind this strategy is to combine the standard lithography with subsequent thermal oxidation to create nanoscale high-aspect-ratio nanochannels. First, channel patterns were defined by standard lithography with a gap size of 0.5–1 mm. Then, the patterns were etched to form narrow, deep trenches by anisotropic KOH etching. Alternatively, the deep reactive ion etching (DRIE) technique was also used to achieve deep trench etching with the Bosch process. To achieve a nanoscale channel, the thermal oxidation process was applied to grow an oxide layer and thereby narrowing the gap down to below 100 nm or even 10 nm. Finally, non-conformal plasma-enhanced chemical vapor deposition (PECVD) oxide deposition was performed to seal the trenches and form vertical nanochannels. This fabrication method is completely CMOS-compatible and does not require any nanolithography or non-conventional fabrication tools.

3.2 Fabrication of nanofluidic concentrators using nonlithographic methods

Even though the preconcentrator devices fabricated in silicon allow solid-state and well-controlled nanochannels, these require extensive micro fabrication steps and, most importantly, the overlapping of the EDL becomes weaker with increasing ionic strength of the buffer system due to the low inherent surface charge of Si/glass. To alleviate these problems, techniques have

been developed to implement electrokinetic concentration schemes in a PDMS microfluidic chip format. PDMS is a widely used material in microfluidics to fabricate the device since it allows a simple replication of the channels. However, fabricating nanochannels in PDMS is challenging due to the elastomeric nature of the material which leads to the collapsing of the nanochannels during or after bonding. A non-traditional way of creating nanochannels is the wrinkling process. When the PDMS surface is exposed to an oxygen plasma while under tensile stress, a stiff skin, largely composed of SiO_x, is formed at the density of which is approximately half that of silica.[28] When slowly released, a sinusoidal wrinkle pattern forms with a well-defined wavelength and an amplitude in the nanometre-scale. Depending on the amount of strain as well as on the exposure duration to the plasma, the amplitude of the wrinkled surface changes between 50–600 nm and its period changes between 100–3500 nm.[29] Alternatively, an ion beam source can be used as a local heat source for wrinkling.[30] To localize the wrinkling to the junction between two microchannels, a transparency film was used to cover the PDMS surface except for the junction area. Using an exposure time of 450 s, a wrinkled nanochannel with a height of 52 nm could be fabricated and used for preconcentration of B-phycoerythrin with a concentration factor of ~10^2.

Another way to create the “nanochannels” without lithographic patterning is the junction gap breakdown method.[31] By applying a high voltage (>1000 V) between two closely adjacent microchannels, nanogaps were formed between microchannels via electrical breakdown. From the dc current measurement, the nanogap size was estimated to be approximately 80 nm in depth. Using this device, a concentration factor as high as 10^4 was achieved for B-phycoerythrin within 1 h. However, the non-reproducible bonding strength between the glass substrate and PDMS chip, as well as limited permselectivity of the nanojunctions, were limiting the yield and efficiency of the preconcentrator device.

3.3 Fabrication of PDMS concentrator using Nafion

Instead of creating the nanochannels on the PDMS device which is challenging because of the softness of the material, one can pattern a submicron thin layer of ion-selective resin on a glass substrate and use this planar membrane as the ion-selective junction between two microchannels.[19] Since the PDMS is flexible, it can easily conform to the shape of the planar layer. The schematic of this Nafion patterning/ printing method is shown in Fig. 7a. In brief, a 5 wt% Nafion perfluorinated ion-exchange resin was patterned by a microflow patterning technique which utilizes the PDMS microchannel reversibly bonded to glass to define the flow path of the resin. After filling the channel with 1 μL of the resin, it was completely flushed out of the microchannel by applying negative pressure on the other end of the channel. After curing at 95 °C for 10 min, the PDMS chip with microchannels was bonded on top of the patterned glass substrate by standard plasma bonding. The SEM analysis revealed a well-defined stripe formed on a glass substrate with a thickness of 191 nm. Alternatively, a thin layer of Nafion resin can be printed on the glass substrate via micro contact printing. The PDMS preconcentration device with an integrated ion-selective Nafion membrane is shown in Fig. 7b. Using this concentrator chip, one could achieve a concentration volume of B-phycoerythrin as high as 200 pL. This was 350-fold larger than that from the silicon/glass device,[3] with a concentration factor as high as ~10^5 within 20 min, as shown in Fig. 7c.

Another useful technique to build a PDMS concentration device is called the “self-sealed” junction method.[20] The self-sealed polymeric nanoporous junction method exploits the softness and flexibility of the PDMS material. Without photolithographical patterning, one can cut the PDMS surface with a knife at the location where a junction is required and infiltrate a low-viscous Nafion resin into the incision after opening the gap through bending.[20] After releasing the PDMS, the trapped Nafion is sealed and cured. In this way, a high-aspect-ratio membrane can be fabricated inside PDMS which enabled a preconcentration with pressure-

driven flow as well as a high sample throughput in large channels with the dimensions of 1000 μm width × 100 μm depth. Instead of cutting the junction, one can also prepattern the junction lithographically and fill it with microbeads and infiltrate Nafion resin into the solid bead matrix which allows a robust perm-selective membrane.[32]

4. Applications

4.1 Immunoassays

The kinetics and sensitivities of immunological reactions and immunoassays are controlled by factors such as antigen concentration, antibody affinity, and diffusion distance (if a heterogeneous assay). Traditional amplification methods, such as that used in enzyme-linked immunosorbent assays (ELISA), improve the sensitivity of assays by increasing the signal generated after the initial binding reactions. While the assay sensitivities can be improved with these post-binding amplification methods or more sensitive detection equipment, the initial binding kinetics remain slow and can become a bottleneck in immunoassays if the concentration of the analytes is low.

The electrokinetic preconcentrator can provide an efficient tool to enhance the binding simply by increasing the concentration of low-abundance analytes. There are two strategies available to integrate the electrokinetic preconcentration into an immunoassay. Firstly, the capture antibody can be immobilized on a flat solid surface using micro contact printing or any standard surface patterning methods. This antibody-immobilized substrate can then be placed on top of a concentrator and seal the microchannel just by adhesion or by mechanical clamping. A common bonding method such as plasma bonding is not applicable since the oxygen plasma would destroy the surface-patterned antibody. Secondly, to achieve higher sensitivity, micro beads can be used instead of flat substrates to immobilize the antibody. The first application of the nanofluidic preconcentrator as an enhancing tool for the immunoassay has been demonstrated with a bead-based assay.[33] The integration concept of the bead-based assay with a nanofluidic preconcentrator is shown in Fig. 8a. Using a depth difference between the deep (12 μm) and shallow (5.5 μm) microchannel, the surface-functionalized micro beads are captured in front of the nanochannels. Then, the sample molecules are concentrated on the antibody-immobilized beads, thus enhancing the immunobinding event. Using a nanofluidic-based concentrator, the sensitivity of the immunoassay for a fluorescent protein, R-phycoerythrin (RPE), was enhanced by more than 500-fold from higher 50 pM to the sub 100 fM range within a 30 min preconcentration with 10 mg mL^{-1} GFP as simulated molecular background, as shown in Fig. 8b. In addition, the detection range of the assay was increased by three orders of magnitude from 10–10 000 ng mL^{-1} to 0.01–10000 ng mL^{-1}. This result shows the potential of the electrokinetic preconcentrator in that it can address the most critical detection issues in the detection of common disease biomarkers.

4.2 Enhanced enzyme assay

Since the lab-on-a-chip (LOC) platform offers advantages relative to microwell plates in analytical speed, performance, reduction of sample/reagent consumption, automation and integration, various types of enzyme activity assays have been implemented in microfluidic chips previously.[34] Still, enzyme assays suffer from low reaction rates if the concentration of enzymes is below the 1 ng mL^{-1} range. One can express the enzyme reaction rate by the Michaelis–Menten equation as below:

$$E+S \underset{k_{-1}}{\overset{k_1}{\rightleftarrows}} ES \xrightarrow{k_2} P \tag{6}$$

$$\frac{d[P]}{dt}(\text{rate of reaction}) = \frac{k_2[E_0][S]}{K_m + [S]} \quad (7)$$

Here, [*P*] denotes the product concentration, [E_0] and [*S*] are the starting amounts of enzyme and substrate concentration, respectively, while k_1, k_{-1}, k_2 are the rate constants for the individual steps. Km is the Michaelis constant which is defined as the concentration where the rate of the enzyme reaction is $V_{max}/2$. V_{max} is the maximum velocity in the reaction rate versus substrate concentration curve. From eqn (7), it is clear that one can increase the reaction rate significantly by increasing the concentrations of enzyme ([E0]) as well as of substrate ([*S*]). Lee et al. demonstrated that an electrokinetic preconcentrator can be used to increase both the reaction rate and the sensitivity of low-abundance enzyme assays (Fig. 9).[35] By using a micro/nanofluidic preconcentration chip and concentrating a mixture of trypsin as enzyme and BODIPY Fl casein as the fluorogenic substrate, the reaction time required to turn over substrates at 1 ng mL^{-1} was only ~10 min compared to ~1 h without preconcentration. Furthermore, trypsin activity could be measured down to a concentration level of 10 pg mL^{-1}, which is an ~100-fold enhancement in sensitivity compared to the result without preconcentration. While this device has significant potential in immunoassays and biosensing applications, it is also clear that any kind of biochemical reaction (not just the binding reaction between antigen and antibody) could be enhanced by concentrating the sample inside this device.

One can apply the same “micro reaction platform” to measure low abundance kinase activities. The use of LOC to measure low abundance kinase activities has not been reported, mainly due to the low abundance of the kinase and its substrate and the low kinase turnover rate. Also, complex, real physiological samples as required for routine applications pose another challenge for measurement. In a PDMS preconcentrator, Lee et al. could perform concentration enhanced cell kinase assays in a micro/nanofluidic platform directly from cell lysates, in order to enable scientific studies on cell signaling pathways at the single cell level.[36] The result showed that a concentration-enhanced enzyme assay with two important cellular kinases, MK2 and PKA from human HepG2 cells, was possible only with lysates from a few cells. This device achieved at least a 25-fold increase in reaction rate and a 65-fold enhancement in sensitivity. The assay time was reduced from ~1 h to 10–20 min as well as the amount of sample was decreased from 200 μL to 5 μL. This reaction-rate enhancing scheme can lead to a quantitative measurement of cellular kinase activities potentially at or near single-cell level, which would give us a deeper and clearer insight into the cellular signal pathways.

4.3 Coupling to droplet-based assay

Electrokinetic preconcentrators allow straining charged species from large volumes (1–10 μL) to very low volume plugs (BpL). However, the concentration plug cannot maintain its final concentration once the voltage is turned off or the plug has to be transported to other locations on the chip for further reactions or analysis. In order to maintain its high concentration for different applications such as enzyme assays, one can encapsulate these plugs of species into water-in-oil droplets and porous gel plugs, as shown in Fig. 10. Droplet-based microfluidics is gaining wide-spread use due to the several advantages such as well-controllable compartmentalization for reactions and excellent fluid handling.[37] Confinement of concentrated enzymes (from the sample) in two-phase droplets is an ideal way to prevent sample dispersion, while allowing the reaction to occur. The advantage of this would be that simpler, Michaelis–Menten reaction models can be applied to extract key reaction parameters from the measurement. Song et al. have coupled the preconcentrator to a two-phase flow channel via a T-junction to encapsulate the sample plug inside a microdroplet with a programmed target concentration.[38] The schematic of the coupled device is shown in Fig. 10a.

Once in the droplets, the molecules as well as nanoparticles such as quantum dots can then undergo biochemical reactions or be delivered anywhere on the chip at the programmed concentration without dispersion losses (Fig. 10b). Using monomers and UV light exposure, even porous solid microparticles were made for easier handling while retaining the set concentration.

5. Concluding remarks

Proper scientific understanding of ICP has been challenging due to the coupled, multi-scale nature of the problem. While traditional model-based prediction and optimization is therefore not possible, several experimental results provide key insights into strategies to improve the device performance further. One of the limiting factors for the concentrator is the fact that the concentration process is not a steady state. As the concentration process progresses, the ion conductivity of the depletion region decreases, making the potential drop and electric field increase. Eventually, the concentration plug becomes unstable, leading to a loss of concentration plug due to unstable flow conditions. Mitigating this instability, mainly resulting from fast and vortex-like nonlinear electrokinetic flow,[10] would be important for future engineering of biomolecule concentration devices. One possible way is decreasing the microchannel depth. The size of the vortical flow follows the depth of the microchannel used. With those suppressed vortices, liquid mixing inside the ion depletion zone is minimized and thus the concentration gradient, which is the driving force of diffusive ion transport, can be maintained in a more stable way.

In addition, since the ICP mechanism is able to block charged molecules only, thus, another concentrating strategy is required for neutral molecules. Since, however, most biomolecules including DNA and proteins have their specific charges at neutral pH value, one can utilize the ICP concentration mechanism for most biomolecules.

The challenges from the fabrication point of view are how to fabricate a robust permselective membrane more reliably and repeatably. A combination of a solid matrix fabricated lithographically with a permselective polymer infiltration would be a promising path to follow. In view of the applications, the challenges the concentrator is facing are how to deal with high ionic strength buffer solutions or the serum samples most of the samples are stored in without losing the permselectivity of the membrane, how to passivate the channel surface without blocking the membrane and how to create a membrane which can survive different types of common solvents even at high voltage in a pressure-driven flow. For successful future applications, a mechanically robust and chemically resistant membrane with high permselectivity would be highly desirable.

Once fully developed, micro/nanofluidic molecular concentration devices can be fabricated and incorporated as a part of integrated microTAS (Total Analysis Systems), functioning as a generic molecular preconcentrator for separation or detection. Given the importance of sample preconcentration in general molecular detection, it is expected that the device will find its place in future, integrated biosensing systems. In addition, the science of ICP can be carefully studied and modeled in the microfluidic molecular concentration device, with its ability to monitor molecular concentration distribution, ion current, and local fluid flow simultaneously.

Acknowledgments

The authors acknowledge various research grants from NSF (CBET-0347348 & 0854026) and NIH (EB005743, CA119402, P50-GM68762) which enabled the works behind this review.

REFERENCES

1. Singh, AK.; Throckmorton, DJ.; Kirby, BJ.; Thompson, AP. Micro Total Analysis Systems. Vol. 1. Kluwer Academic; Nara, Japan: 2002. p. 347-349.
2. Foote RS, Khandurina J, Jacobson SC, Ramsey JM. Anal. Chem 2005;77:57–63. [PubMed: 15623278]
3. Wang Y-C, Stevens AL, Han J. Anal. Chem 2005;77:4293–4299. [PubMed: 16013838]
4. Lichtenberg J, Verpoorte E, Rooij N. F. d. Electrophoresis 2001;22:258–271. [PubMed: 11288893]
5. Cui H, Horiuchi K, Dutta P, Ivory CF. Anal. Chem 2005;77:7878–7886. [PubMed: 16351133]
6. Jung B, Bharadwaj R, Santiago JG. Anal. Chem 2006;78:2319–2327. [PubMed: 16579615]
7. Oleschuk RD, Shultz-Lockyear LL, Ning Y, Harrison DJ. Anal. Chem 2000;72:585–590. [PubMed: 10695146]
8. Song S, Singh AK, Kirby BJ. Anal. Chem 2004;76:4589–4592. [PubMed: 15283607]
9. Khandurina J, Jacobson SC, Waters LC, Foote RS, Ramsey JM. Anal. Chem 1999;71:1815–1819. [PubMed: 10330910]
10. Kim SJ, Wang Y-C, Lee JH, Jang H, Han J. Phys. Rev. Lett 2007;99:044501. [PubMed: 17678369]
11. Probstein, RF. Physicochemical Hydrodynamics : An Introduction. Wiley-Interscience; 1994.
12. Holtzel A, Tallarek U. Journal of Separation Science 2007;30:1398–1419. [PubMed: 17623420]
13. Mao P, Han J. Lab Chip 2005;5:837–844. [PubMed: 16027934]
14. Mao P, Han J. Lab Chip 2009;9:586–591. [PubMed: 19190794]
15. Pu Q, Yun J, Temkin H, Liu S. Nano Lett 2004;4:1099–1103.
16. Mani A, Zangle TA, Santiago JG. Langmuir 2009;25:3898–3908. [PubMed: 19275187]
17. Jin X, Joseph S, Gatimu EN, Bohn PW, Aluru NR. Langmuir 2007;23:13209–13222. [PubMed: 17999544]
18. Kim SJ, Li L, Han J. Langmuir 2009;25:7759–7765. [PubMed: 19358584]
19. Lee JH, Song Y-A, Han J. Lab Chip 2008;8:596–601. [PubMed: 18369515]
20. Kim SJ, Han J. Anal. Chem 2008;80:3507–3511. [PubMed: 18380489]
21. Dhopeshwarkar R, Crooks RM, Hlushkou D, Tallarek U. Anal. Chem 2008;80:1039–1048. [PubMed: 18197694]
22. Rubinstein I, Zaltzman B. Phys. Rev. E 2000;62:2238–2251.
23. Ben Y, Chang H-C. J. Fluid Mech 2002;461:229–238.
24. Rubinstein SM, Manukyan G, Staicu A, Rubinstein I, Zaltzman B, Lammertink RG, Mugele F, Wessling M. Phys. Rev. Lett 2008;101:236101. [PubMed: 19113567]
25. Zaltzman B, Rubinstein I. J. Fluid Mech 2007;579:173–226.
26. Daiguji H, Yang P, Majumdar A. Nano Lett 2004;4:137–142.
27. Huang K-D, Yang R-J. Microfluidics and Nanofluidics 2008;5:631–638.
28. Mahadevan L, Matsudaira P. Science 2000;288:95–99. [PubMed: 10753126]
29. Chung S, Lee JH, Moon M-W, Han J, Kamm RD. Advanced Materials 2008;20:3011–3016.
30. Moon M-W, Lee SH, Sun JY, Oh KH, Vaziri A. Proc. Natl. Acad. Sci. U. S. A 2007;104:1130–1133. [PubMed: 17227839]
31. Lee JH, Chung S, Kim SJ, Han J. Anal. Chem 2007;79:6868–6873. [PubMed: 17628080]
32. Song Y-A, Batista C, Sarpeshkar R, Han J. J. Power Sources 2008;183:674–677.
33. Wang Y-C, Han J. Lab Chip 2008;8:392–394. [PubMed: 18305855]
34. Kerby MB, Legge RS, Tripathi A. Anal. Chem 2006;78:8273–8280. [PubMed: 17165816]
35. Lee JH, Song Y-A, Tannenbaum SR, Han J. Anal. Chem 2008;80:3198–3204. [PubMed: 18358012]
36. Lee JH, Cosgrove BD, Lauffenburger DA, Han J. J. Am. Chem. Soc 2009;131:10340–10341. [PubMed: 19722608]
37. Song H, Chen DL, Ismagilov RF. Angew Chem Int Edit 2006;45:7336–7356.
38. Song, Y-A.; Sarkar, A.; Han, J. MicroTAS 2008. San Diego, CA: 2008.

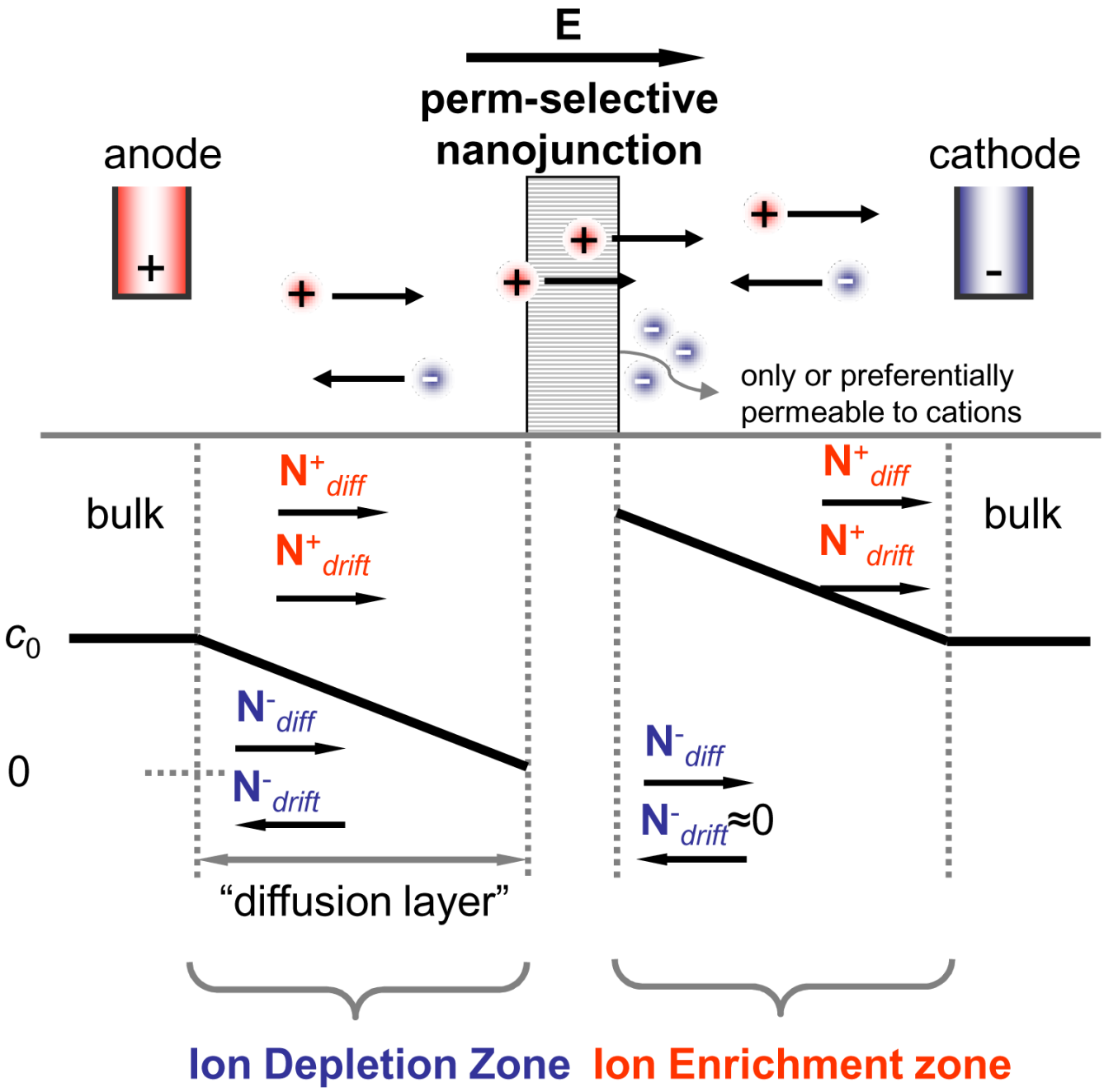

Figure 1.

Schematic diagram of ion concentration distribution at the front and back of a cation perm-selective nanostructure which only lets cations pass through. N^+ and N^- are the fluxes of cation and anion, respectively, and the subscripts *diff* and *drift* represent the diffusive and drift ion transport, respectively. **E** is the applied electric field across the membrane.

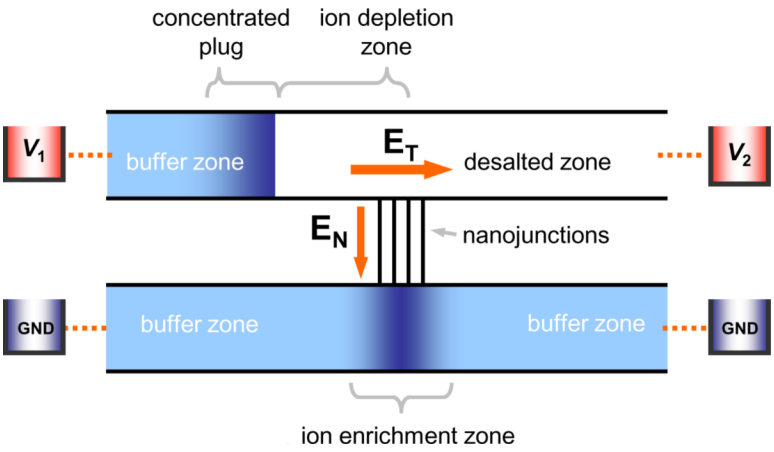

Figure 2.
Schematic diagram of a single-gated electrokinetic concentrator in a typical micro/nanofluidic hybrid channel system and electrical configurations under dc bias.

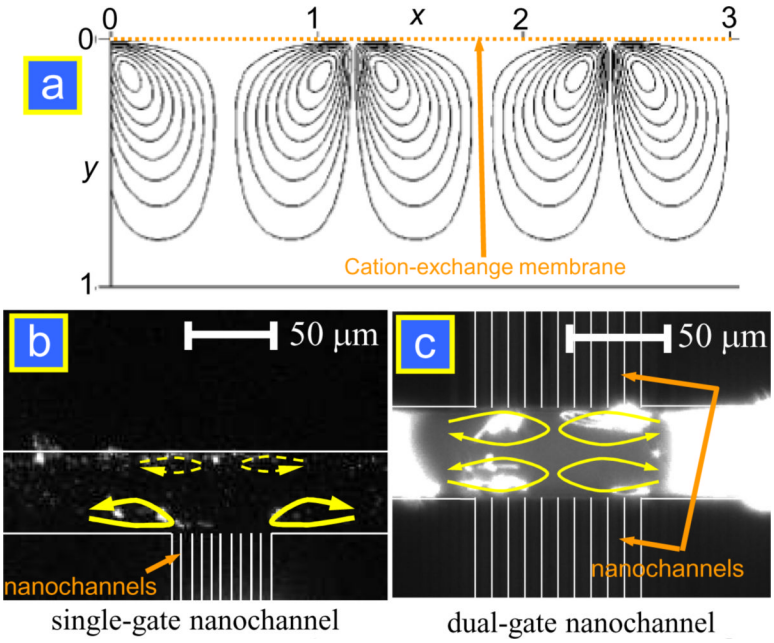

Figure 3.

(a) Mathematically calculated steady state streamline near perm-selective membrane located at $y = 0$. (b) Snapshots of tracer particles at different applied voltages showing quasi-steady state streamlines near cation-exchange membrane. (c) Fast vortices in single-gated micro/nanofluidic device. (d) Since the ions were depleted through nanochannels on both sides, four independent vortices were formed in the four divided regions in a dual-gated device. Reprinted with permission from (a) [ref. 22], (b) [ref. 24] and (c), (d) [ref.10].

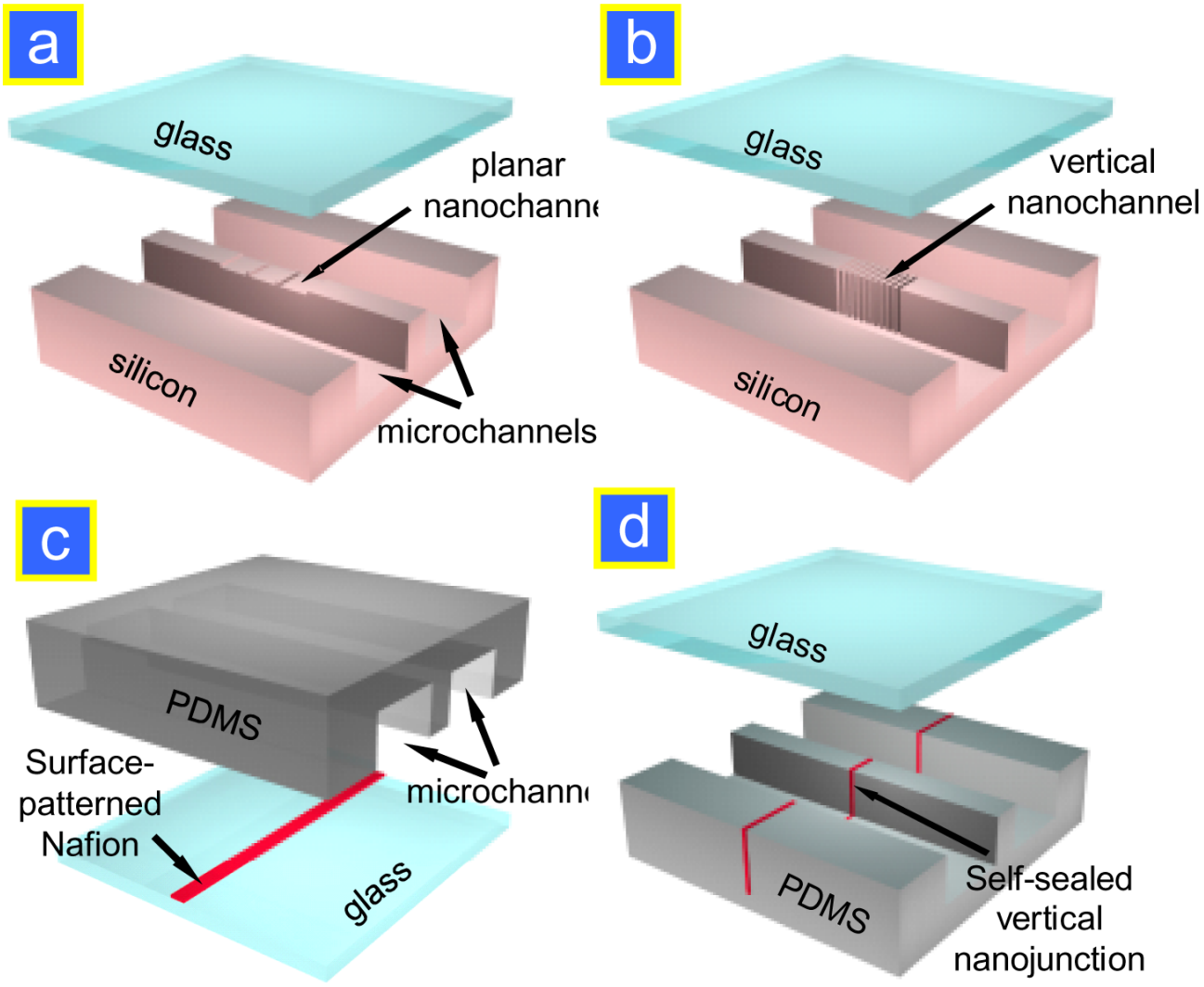

Figure 4.
Available techniques for fabricating perm-selective nanojunctions. (a) Planar nanochannel fabrication in Si/glass.[13] (b) Vertical nanochannels in Si.[14] (c) Surface-patterned Nafion junction.[19] (d) Self-sealed Nafion junction.[20]

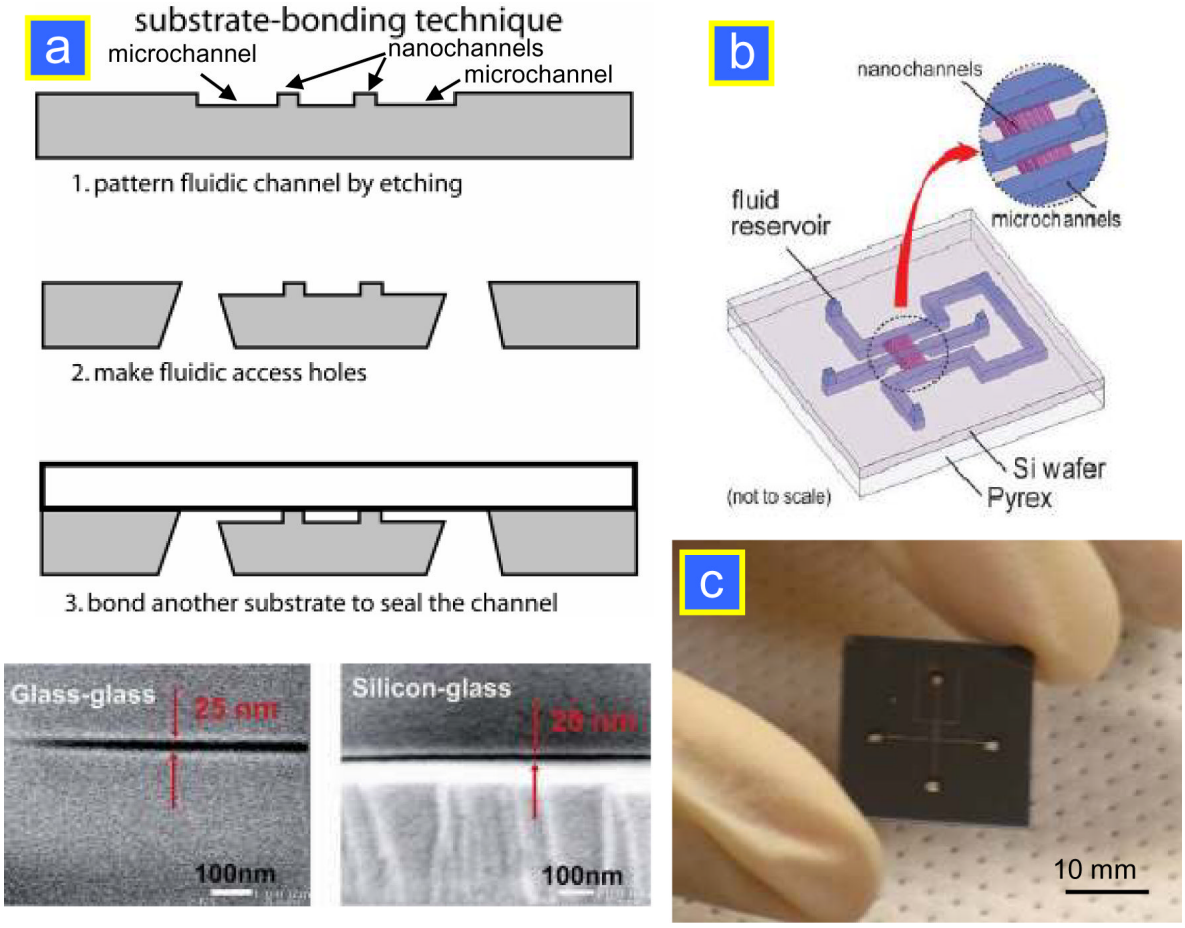

Figure 5.

Schematic diagram of the (a) device fabrication[13] and (b) nanofluidic biomolecule concentrator.[33] For the device fabrication, only standard lithography was required. A nanoscale channel depth down to 20 nm can be fabricated and sealed by anodic bonding without collapsing. (c) The dual-gated preconcentrator chip in silicon-glass.

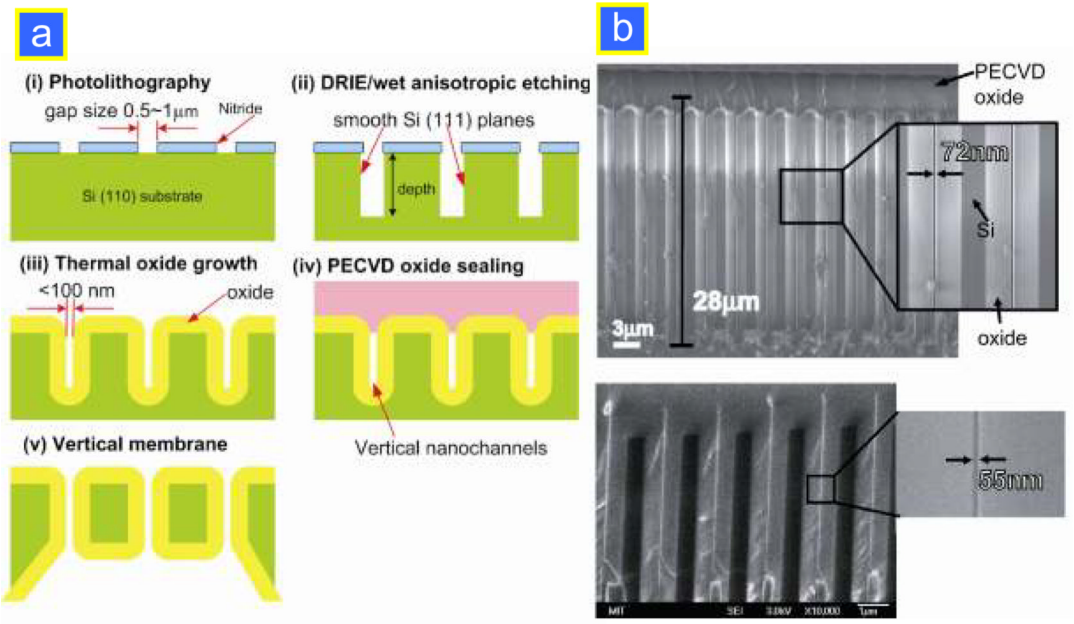

Figure 6.

(a) Schematic diagram of fabricating vertical nanochannels:[14] (i) photolithography defines pattern structures; (ii) vertical trenches with smooth sidewalls are etched by either DRIE or anisotropic wet etching (KOH); (iii) thermal oxide growth further decreases the gap size; (iv) uniform PECVD oxide is deposited to seal narrow trenches; (v) backside etching of the Si wafer yields thin membranes over a wide area (~6 inch wafers). (b) Cross-sectional SEM micrographs of slot-like vertical nanochannels with a uniform gap size of 72 nm and 55 nm. The channels are etched by KOH etching and have a depth of 28 μm. The channels are completely sealed by depositing 3 μm thick PECVD oxide.

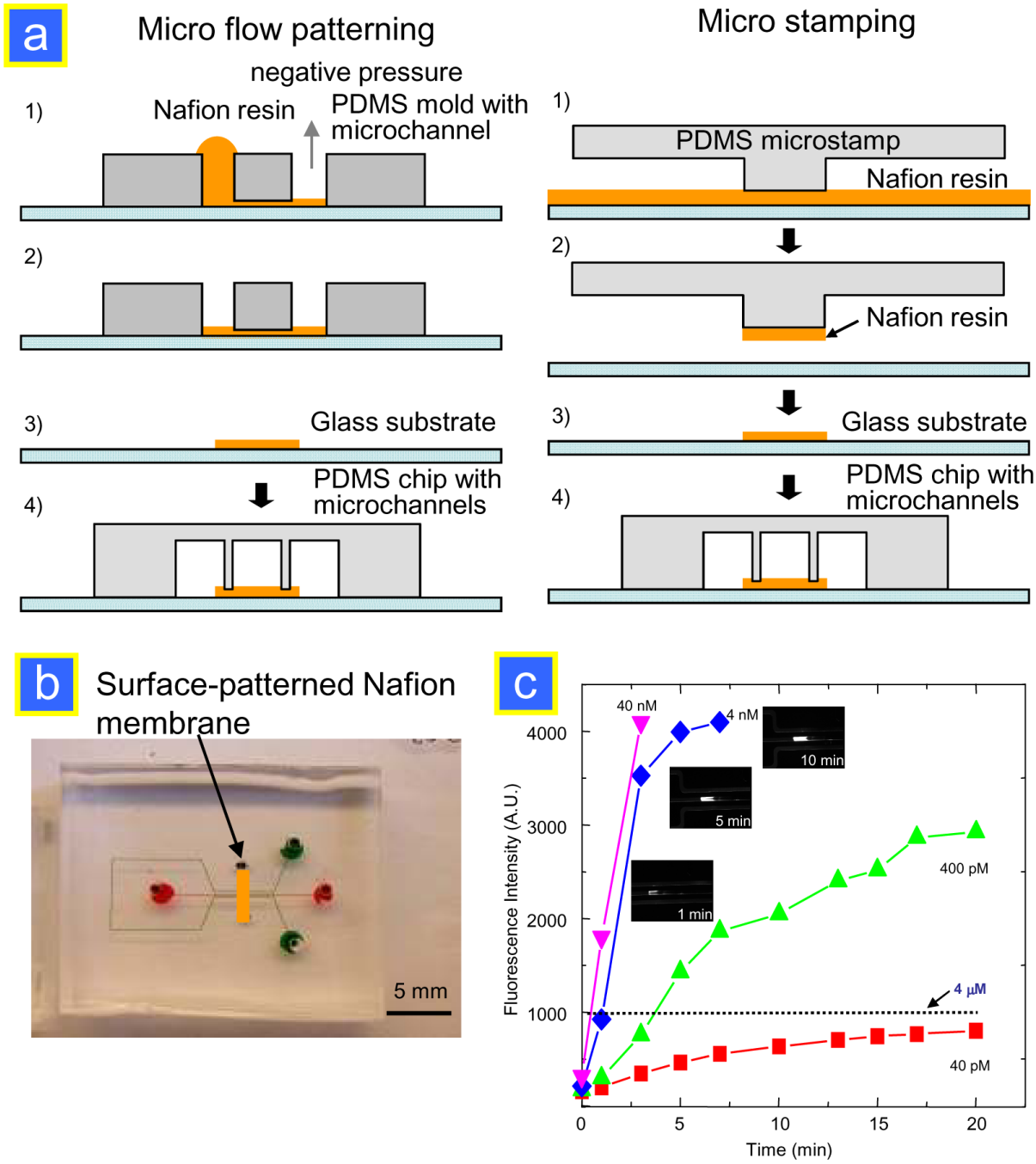

Figure 7.

(a) Schematic of the micro flow patterning and micro contact printing techniques to pattern a planar Nafion membrane on a glass substrate.[19] (b) PDMS preconcentrator chip with surface-patterned ion-selective membrane.[19] (c) Preconcentration of β-phycoerythrin versus electrokinetic trapping time. This result shows that one can achieve a preconcentration factor of ~10^5 in 20 min. Fluorescence images of 4 nM protein shown next to the graph prove an increase in the concentrated plug in size and concentration with trapping time.[19]

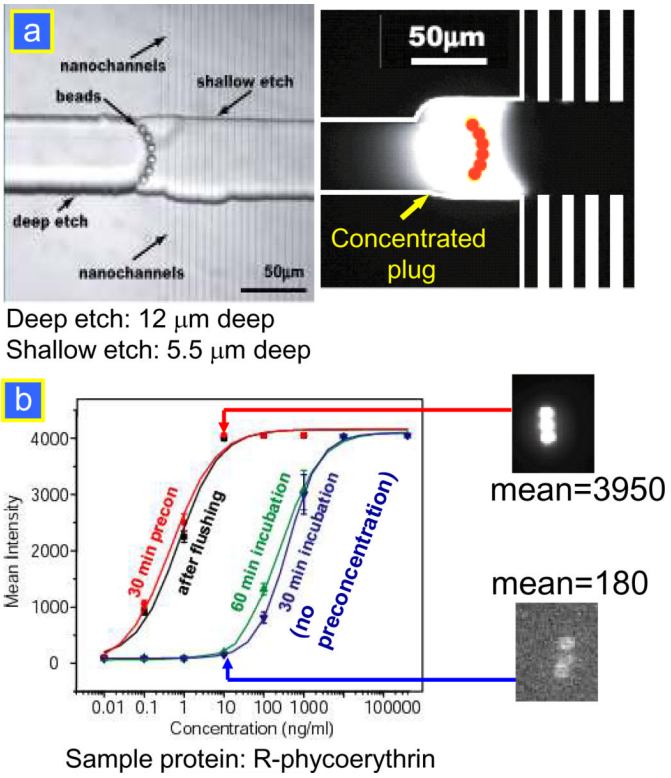

Figure 8.

(a) Integration concept of bead-based assay and nanofluidic preconcentrator. Trapped beads at the weir structure in front of the nanochannels.[33] (b) Immunosensing without and with preconcentration in a nanofluidic bead-based assay. The enhanced signals (bound RPE on the beads) were not affected by the additional washing/flushing step, clearly demonstrating the enhanced binding by the preconcentration step.[33]

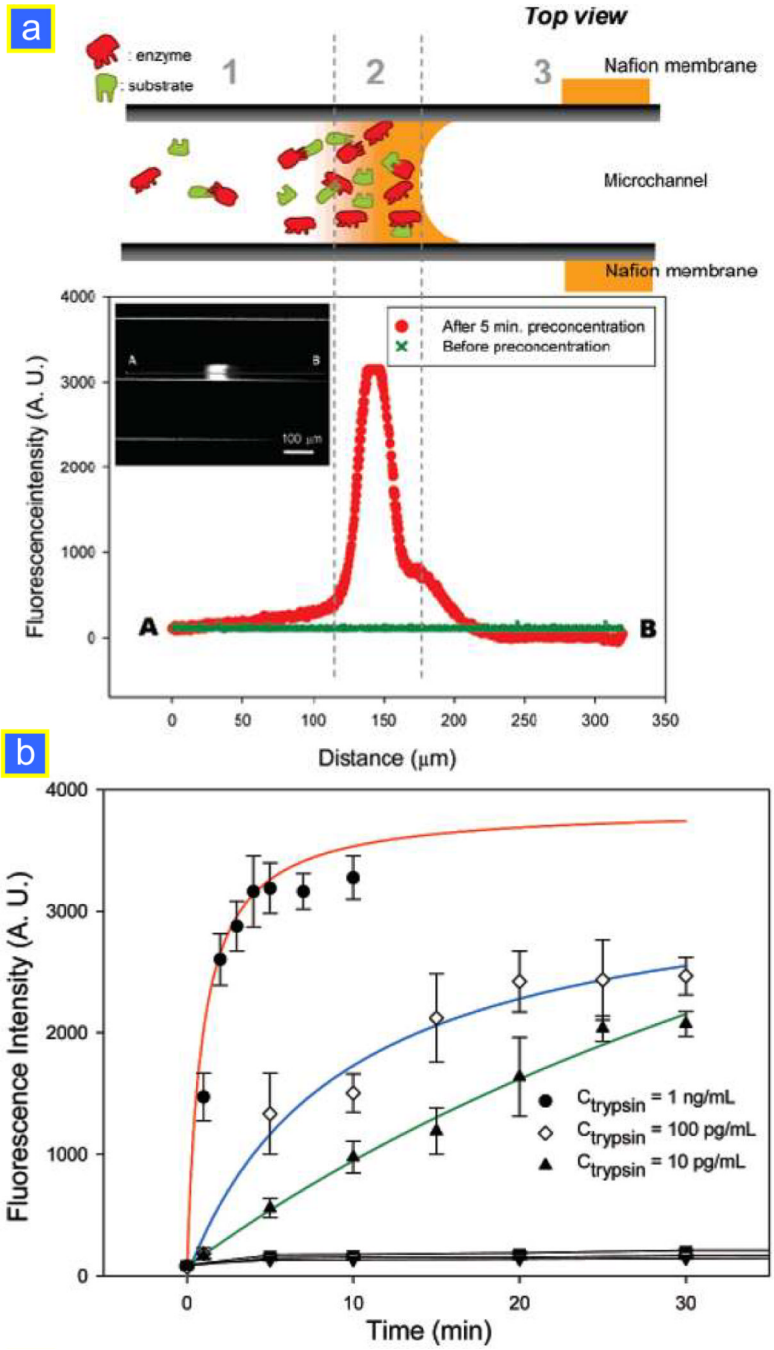

Figure 9.

(a) Scheme and product profile from the enzyme–substrate reaction, showing the enhancement of enzyme–substrate turnover rate at the concentrated zone generated by nanofluidic electrokinetic trapping. When preconcentration operated, enzyme as well as substrate is concentrated near the nanochannel (zone 2), consequently enhancing the reaction kinetics of a low abundant enzyme. Zone 1 indicates the reaction in a microchannel in the zone far from the concentrating zone. The difference in fluorescence signals from zone 1 and 2 means enhancing enzyme activity by the preconcentrating operation. Zone 3 illustrates the depletion zone, showing the control experiments for eliminating background noise that can be generated from the adsorption of enzyme/substrate. (b) Fluorescence intensity of products with the

preconcentration operation, showing the enhancement of the trypsin catalyzed reaction with preconcentration. Reprinted with permission from [ref.35].

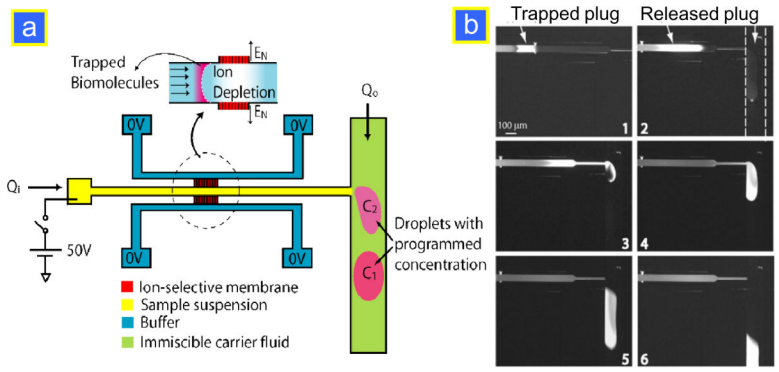

Figure 10.

(a) Microencapsulation of molecules with variable concentration is realized by combining an electrokinetic preconcentrator with droplet generation in immiscible fluid via a T-junction. (b) This sequence demonstrates how the concentrated FITC sample was encapsulated in immiscible fluid: 1. electrokinetic trapping of the sample in the preconcentrator at V_{high} = 500 V; 2. the release of the concentrated plug after 5 min preconcentration; 3. the concentrated sample is being injected into the immiscible mineral oil with the pressure-driven flow via a T-junction; 4. the sample plug is completely encapsulated in the droplet; 5. break-off of the droplet from the T-junction; 6. dispersion-free transport of the concentrated sample plug along the microchannel. Reprinted with permission from [ref.38].

Table 1

Comparison of available fabrication strategies for nanojunctions

	Ease of fabrication	Mechanical strength	Reusability	Permselectivity
a. Planar	++	+++	+++	+
b. Vertical	+	+++	+++	++
c. Surface-patterned	+++	+	+	+++
d. Self-sealed	+++	+	+	+++